Membrane interactions control residue fluctuations of outer membrane porins

A. B. Besya,[1] H. Mobasheri,[2] and M. R. Ejtehadi[3,*]
[1]*Institute for Nano Science and Technology, Sharif University of Technology, P.O. Box 14588-89694, Tehran, Iran*
[2]*Laboratory of Membrane Biophysics, Institute of Biochemistry and Biophysics, University of Tehran, P.O. Box 13145-1384, Tehran, Iran*
[3]*Department of Physics, Sharif University of Technology, P.O. Box 11155-9161, Tehran, Iran*
(Received 5 October 2009; revised manuscript received 3 March 2010; published 11 May 2010)

Bacterial outer membrane porins (Omp) that have robust β-barrel structures, show potential applications for nanomedicine devices in synthetic membranes and single molecule detection biosensors. Here, we explore the conformational dynamics of a set of 22 outer membrane porins, classified into five major groups: general porins, specific porins, transport Omps, poreless Omps and composed pores. Normal mode analysis, based on mechanical vibration theory and elastic network model, is performed to study the fluctuations of residues of aforementioned porins around their equilibrium positions. We find that a simple modification in this model considering weak interaction between protein and membrane, dramatically enhance the stability of results and improve the correlation coefficient between computational output and experimental results.

DOI: 10.1103/PhysRevE.81.051911 PACS number(s): 87.15.−v, 36.20.−r, 02.70.−c, 46.15.−x

I. INTRODUCTION

Membrane proteins are a broad class of protein, which are partially or fully associated with cellular membranes. They are characterized by their rich dynamical properties and are known to be responsible for mediating the exchange of ions, molecules, and information across cellular boundaries [1]. Porins are integral membrane proteins that are found in the outer membrane of Gram-negative bacteria, eukaryotic mitochondria and chloroplasts. The Omps, according to their functions and structure can be subdivided into the five groups of Table I [2]. The general porins, yielded the first x-ray-grade membrane-protein crystals [3], function as water-filled transport channels that allow for diffusion of small polar molecules roughly up to 600 Daltons [4–8]. Their hollow structures are composed of 16 antiparallel β strands connecting with loops that are responsible for channel peculiarities and that can evolve without strong structural constraints. The next group that are closely related structurally to the general porins, are specific porins composed of 18 antiparallel β-strands. Three internal loops constrict the channel of these porins to a minimal diameter of only 5 Å [9–11]. The third group of Omps, transport Omps, have much larger β-strands and additional internal domains which may work as a stopper. They are not likely to form a pore, but open and close for the passage of large molecules such as iron-containing siderophores or cobalamins through the outer membrane [12–15]. Poreless Omps contain small β strands that function as membrane anchors and fulfill numerous purposes using their extracellular and periplasmic surfaces. Their small β barrel has a nonpolar exterior and polar interior, and therefore can be considered as inverse micelles [16–21]. Finally, a quite different group is composed of nanopores where the β barrel itself is a homo-oligomer, a heptamer in α-hemolysin [22], and a trimer in TolC [23]. Although Omps as nanopores appear to have a relatively simple structure, they exhibit interesting properties. They may be used in many applications such as nanomedicine devices in synthetic membranes and biosensors [24–26].

Recent studies show that, owing to the intrinsic structural flexibility of macromolecules such as proteins and nucleic acids, they generally possess a tendency to adjust their three-dimensional conformation to enable their biological functions associated [27]. Examining the protein structural flexibilities can provide valuable information about their structure-function relationships. Molecular dynamic (MD) simulations are powerful yet time consuming tools for atomic scale studies. On the other hand, normal mode analysis (NMA), which is an efficient method for identifying functional motions of proteins, has been utilized widely to characterize molecular fluctuations near the equilibrium states [28]. Recently, a broad overview of normal mode analysis has been presented and the applications of this technique have been explored in the study of biological systems [29,30].

Elastic network models (ENM) are known as a simple yet powerful models to perform normal mode analyses for proteins [31]. To reduce the computational cost, coarse-grained approaches have later been implemented into the ENM to study the fluctuation dynamics of a protein around its native conformation [32]. In this model a protein molecule is represented by a network of linear springs and the sophisticated semiempirical potentials are replaced by a single-parameter harmonic potential.

In this paper, normal mode analysis based on mechanical vibration theory and elastic network models is performed to investigate the fluctuation dynamics of outer membrane porins around their equilibrium state. In modeling the elastic network we only consider the C_α atoms and treat them as point masses linked by harmonic springs. We also show that a simple modification of elastic networks considering interactions between membrane and barrel residues based on a modification for MD simulations proposed by Watanabe *et al.* to study the structure and dynamics of the *Escherichia coli* OmpF porin [33] improves the numerical results to correlate well with crystallographic experimental results.

*Author to whom correspondence should be addressed; ejtehadi@sharif.edu

TABLE I. Simulation results for available structures of bacterial outer membrane porins all of which consist of β barrels.

Porin type	Organism	PDB code	N_β [a]	c_b/c	r_c(Å)	Δ_{SD} [b]	$\Delta_{SD,C}$ [c]	$r_{\max}$ [d]	$r_{\max,C}$ [e]	Reference
General porins										
Rc-porin	Rhodobacter capsulatus	2POR	16	0.003	11	0.16	0.03	0.59	0.69	[4]
OmpF	*E. coli*	2OMF	16	0.002	7	0.04	−0.02	0.62	0.72	[5]
PhoE	*E. coli*	1PHO	16	0.002	11	0.14	0.0	0.38	0.62	[5]
Rb-porin	Rhodobacter blasticus	1PRN	16	0.0	9	0.05		0.82		[6]
OmpK36	Klebsiella pneumoniae	1OSM	16	0.005	12	0.25	−0.01	0.64	0.76	[7]
Omp32	Comamonas acidovorans	1E54	16	0.003	8	0.2	0.09	0.6	0.86	[8]
Specific porins										
LamB	*E. coli*	1MAL	18	0.005	8	0.24	0.1	0.7	0.86	[9]
LamB	Salmonella typhimurium	1MPR	18	0.006	8	0.3	−0.05	0.89	0.92	[10]
ScrY	S. typhimurium	1OH2	18	0.0	12	0.09	0.0	0.73		[11]
Transport Omps										
FhuA	*E. coli*	1BY3	22	0.001	8	0.36	0.09	0.6	0.7	[12]
FepA	*E. coli*	1FEP	22	0.007	8	2.24	0.17	0.48	0.62	[13]
FecA	*E. coli*	1KMO	22	0.001	8	0.14	0.03	0.67	0.75	[14]
BtuB	*E. coli*	1NQH	22	0.001	8	0.15	0.05	0.29	0.39	[15]
Poreless Omps										
OmpA	*E. coli*	1BXW	8	0.001	7	0.34	0.0	0.26	0.35	[16]
OmpX	*E. coli*	1QJ8	8	0.008	8	0.35	0.09	0.64	0.68	[17]
OmpLA	*E. coli*	1QD5	12	0.004	11	0.31	0.11	0.37	0.44	[18]
OmpT	*E. coli*	1I78	10	0.005	9	0.36	0.1	0.67	0.78	[19]
OpcA	Neisseria meningitidis	1K24	10	0.001	10	0.44	−0.11	0.25	0.86	[20]
NspA	N. meningitidis	1P4T	8	0.006	9	0.16	−0.23	0.42	0.43	[21]
Composed pores										
α-hemolysin	Staphylococcus aureus	7AHL	14	0.0	10	0.13		0.83		[22]
TolC	*E. coli*	1EK9	12	0.0	12	0.1		0.73		[23]

[a]Number of β-strands
[b]Difference between standard deviation of experimental data and simulation result for unconstrained ENM
[c]Difference between standard deviation of experimental data and simulation result for constrained ENM
[d]maximum correlation coefficient for unconstrained ENM
[e]maximum correlation coefficient for constrained ENM

II. METHODS

In a coarse-grained ENM the protein is represented by a network of selected point masses linked together with harmonic springs that represent the interactions between residues, both the chemical (protein backbone) and physical bonds. In our model only C_α atoms were considered as point masses. The resultant structure from elastic network model resembled a complex mechanical truss. Although it has been shown that many-body interactions may improve the dynamics of the system [34], we only considered pair-contact potentials to construct the elastic network of the protein. For example, the secondary structure of an OmpF monomer and its corresponding elastic network are shown in Fig. 1, respectively.

NMA, based on mechanical vibration theory, is commonly employed in studying large-amplitude molecular deformational motions [35]. The total kinetic energy in a network of n point masses has the form

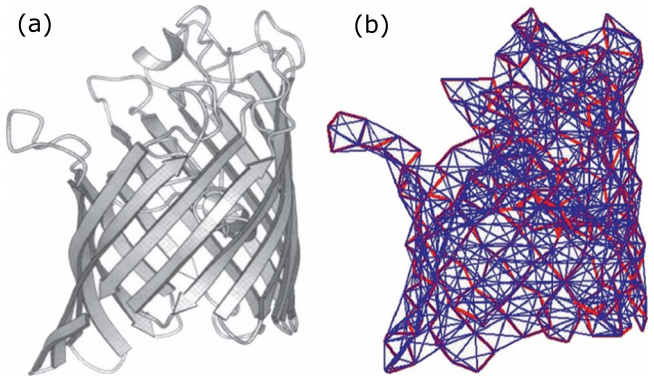

FIG. 1. (Color online) OmpF porin structure (a) Native structure of OmpF porin. Just one monomer is shown. (b) Elastic network model of OmpF porin in the same view of Fig. 7(a).

$$T = \frac{1}{2}\sum_{i=1}^{n} m_i |\dot{\vec{x}}(t)|^2, \quad (1)$$

where, $\vec{x}(t)$ is the position at time t and m_i is the mass of the ith atom. On the other hand, the total potential energy in a network of connected springs has the form

$$V = \frac{1}{2}\sum_{i=1}^{n-1}\sum_{j=i+1}^{n} k_{ij}[|\vec{x}_i(t) - \vec{x}_j(t)| - |\vec{x}_i(0) - \vec{x}_j(0)|]^2, \quad (2)$$

where, k_{ij} is the spring constant between masses i and j, and $t=0$ refers to the initial (equilibrium) positions.

Having the kinetic and potential energies, the equations of motion was derived from the Lagrange equation. Solving the generalized eigenvalue problem, the eigenvalues and their eigenvectors related to the frequencies and the directions of corresponding modes were derived, respectively, [35] and natural modes were calculated.

The structure of outer membrane porins were obtained from the Protein Data Bank. Computations were performed on the assembled subunit structures, for example, trimeric structure for OmpF, monomeric subunit for OmpA and heptameric structure for α-hemolysin. First, a stiffness matrix for the protein was constructed according to the aforementioned coarse-grained protein elastic network model. All C_α's closer than a cut-off distance r_c, were connected by harmonic springs. To further simplify our model, we use an equal mass, m, for each point particle disregarding the size differences in the amino acids. All harmonic springs have the same stiffness, c, with given free lengths equal to the distance between corresponding C_α's in the native configuration. That means

$$k_{ij} = \begin{cases} c & |\vec{x}_i(0) - \vec{x}_j(0)| < r_c \\ 0 & \text{otherwise} \end{cases}. \quad (3)$$

Note that the cut-off distance, r_c, depends on both the nature of the interactions between heavy atoms and the geometry of the interacting residues [36]. The contact between two residues can be defined by the number of bonds or the interactions between heavy atoms [37]. Here, we found it more convenient to indicate the contact between two residues by the distance between the nodes.

The B factor of residue i,

$$\beta_i = 8\pi^2 \langle |\vec{\delta}_i|^2 \rangle, \quad (4)$$

where $\delta_i(t)$ is the displacement vector, are measurable quantities (e.g., Debye-Waller temperature factor in x-ray crystallography experiments) [35], and have often been used as a probe for verifying and improving computational models [36]. Solving the related eigenvalue equation in the elastic network model allows us to compute B-factors for each node. If the kth lowest mode is given by

$$\vec{\nu} = [(\vec{s}_k^{\,1})^T, (\vec{s}_k^{\,2})^T, \ldots, (\vec{s}_k^{\,n})^T]^T, \quad (5)$$

where $\vec{s}_k^{\,i}$ is the ith component of the kth eigenvector of stiffness matrix, the B factors can be described by the expected residue fluctuations as [35]

$$V = \frac{8\pi^2 k_B T}{c}\sum_{k=1}^{3n} \frac{|\vec{s}_k^{\,i}|^2}{\lambda_k}. \quad (6)$$

Here λ_k is the kth lowest eigenvalue of stiffness matrix that is related to the frequency of the corresponding normal mode by $\lambda_k = \omega_k^2$.

From the calculated B factor, the time average of the deviation from the reference position (mean square fluctuations) of residue i can be estimated via,

$$\langle \Delta r_i^2 \rangle = \frac{3\beta_i}{8\pi^2}. \quad (7)$$

III. RESULTS

From the normal mode analysis using elastic network model, mean square fluctuations of the residues of several groups of membrane proteins are calculated. The calculated numerical results have been scaled such that the areas under the simulation result and crystallographic experimental result become equal in order to compute the spring constant [spring constant is shown by symbol c in Eq. (6)] [35]. In this way, the spring constant depends on the cut-off radius (r_c) which is the maximum possible distance between two interacting residues. Increasing the cut-off radius increases the number of model springs. Here, we describe the results for all groups of outer membrane porins.

A. General porins

General porins are the most abundant species of outer membrane proteins. All structurally known proteins in this group are trimers formed by monomers consisting of 16 stranded β barrels as indicated in Table I. All strand axes are approximately perpendicular to the membrane plane, and they function as channels. OmpF as a first structurally established membrane protein and its homologs, PhoE and OmpK36, are somewhat special as their barrel axes deviate by about 10° from the membrane normal [2]. We use OmpF as the representative of this group to show the details of numerical result and then we summarize the results for all porins in Table I.

Figure 2 compares the experimental mean square fluctuations with our calculated values for OmpF porin. The spring constant in Fig. 2, where $r_c = 7.0$ Å has been used, was obtained to be about 7.1 kcal/(mol.Å^2). The calculated correlation coefficient in Fig. 2 is 0.62 which indicates a relatively high correlation between the model and experiment. Our numerical results properly distinguished between flexible residues and rigid ones, nevertheless these differences were exaggerated in calculated results when compared to experimental data. In addition, the correlation with our results and experiment does not improve more when different cut-off values are selected. This is, in fact, the best correlation we could attain for the range of cutoffs that we have inspected.

We will show shortly that one of the reasons for the discrepancies between our results and the experiment is overlooking the interactions between the bilayer membrane and

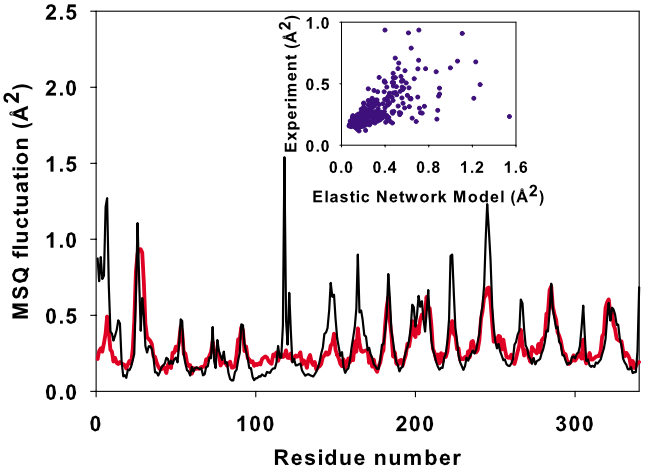

FIG. 2. (Color online) Mean square fluctuations, $\langle \Delta r_i^2 \rangle$, for unconstrained elastic network model with r_c=7.0 Å (dark black line) and the experimental values (light red line). Two sets of data (inset) show a correlation of r=0.62.

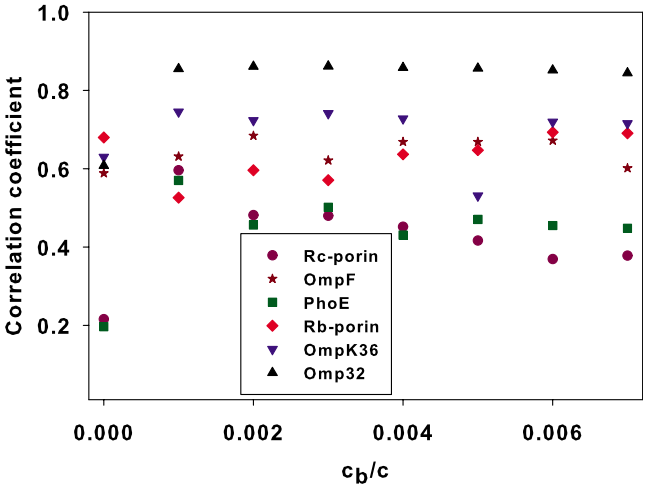

FIG. 3. (Color online) The correlation coefficient between the x-ray experimental data and the constrained elastic network model calculations of mean square fluctuations for general porins at different spring constant ratios. The cut-off distance was taken 8.0 Å in the calculations.

proteins. These interactions have already been shown to be critical in refolding OmpF proteins [38,39]. It has also been shown in MD simulations of the OmpF porin by Watanabe *et al.* that considering a very weak harmonic constraint on the outer portion residues not only stabilizes the porin structure but also improves the prediction of average fluctuations [33]. The outer portion of general porin trimer is where the protein is in contact with the lipid bilayer.

Even though, the crystal structure of proteins is constrained itself [40], for considering interaction between bilayer membrane and outer portion of membrane protein, we impose additional springs to the outer portion of Omps. In this constrained model (unconstrained model means the model without the additional springs for considering membrane interaction) springs with spring constant c_b, connect each node in the outer portion of Omps to a virtual stationary node on the barrel axis having the identical z coordinate. This region includes 8β strands that starts from β7 and goes through β14. Just like Watanabe *et al.* [33], we observed that these springs were, by a few orders of magnitude, softer than the springs connecting the rest of residues. However, this small modification in the model significantly improves the results.

At the equilibrium state the head groups of membrane lipids are immobile/stationary, while, continuous conformational changes occur at the acyl chain area, that cause lateral pressure on nearby channel [41]. Here, we try to measure this lateral pressure exerted on channel wall as membrane-protein interaction. These interactions are much weaker than what was reported as lipid-protein interactions inferred from lipid-protein binding assays and protein extraction from lipid that include head group-protein interactions, counteracting against the effect of counterions. Also, part of the energy involved in these reportedly strong interactions is consumed for solvation of lipid, which in not the case in our study. In spite of the central role of membrane-protein interactions in membrane-protein functions, these interactions are poorly understood.

To estimate the lateral pressure between membrane and protein, a thermodynamic model has been proposed by Cantor [41] based on the hypothesis that variation in membrane composition induces changes in a transverse pressure profile in the lipid bilayer. They found a value of γ=0.05 N/m for lateral pressure exerted on the outer wall of the membrane protein. In our study, we found that the best consistency with experiment came from calculation of the mean square fluctuations with a cut-off value of 7.0 Å (Fig. 4) and a constant c_b=0.002c, which was c_b=0.0142 kcal/mol.Å^2 for the harmonic potential of constraint spring. The value of the spring constant implemented in our study is very close to the value reported in the MD studies of Watanabe *et al.* [33]. Here, we have tried to use this value to estimate the lateral pressure imposed on the channel. The effective spring constant we have found is close to the lateral pressure estimated by Cantor [41], and much lower than the value for protein-lipid interactions reported based on dissociation experiments.

Figure 3 shows the correlation coefficient dependence on the value of the constraint spring constant for general porins at a cut-off value of 8.0 Å. This figure shows that c_b =0.002c improves the correlation coefficient for 83% of porins in this group and the average of the values of best c_b for each porin in this group is 0.0025c. Also, introducing these springs in the ENM, decreases the difference between the standard deviation of experimental data and simulation results in the constrained network. Even though, these proteins are in the same family, the result shows notably different values. This result is related to the difference in the elastic networks for them. For example, OmpF and PhoE have a 3% difference in the number of residues but the difference in sequence is 37.9% (calculated by FASTA program [42]) and in the best alignment their corresponding elastic networks overlap only by 55%. Moreover, their experimentally measured temperature factors from their protein data bank (PDB) file show notably different values that could be the effect of the differences in sequence and the differences in their elastic networks.

In both constrained and unconstrained models the results were sensitive to the choice of the cutoff. However, when

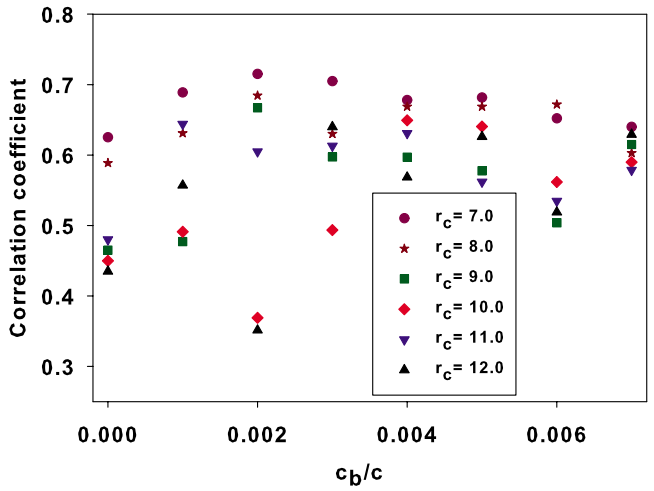

FIG. 4. (Color online) The correlation coefficient between calculated mean square fluctuations of OmpF residues for different cut-off distances.

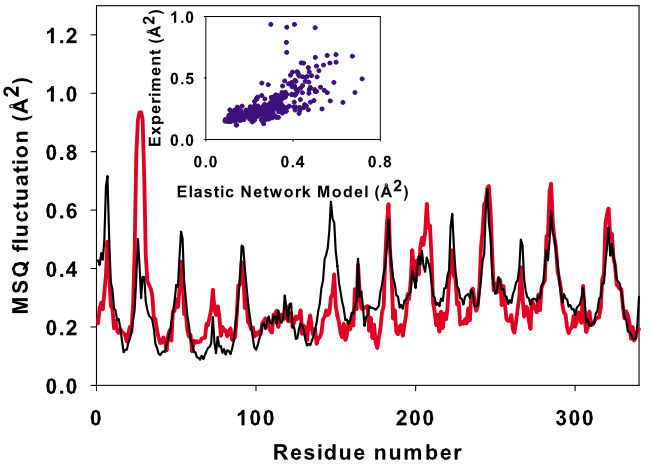

FIG. 6. (Color online) Mean square fluctuations, $\langle \Delta r_i^2 \rangle$, for a constrained elastic network model with r_c=7.2 (dark black line) and the experimental values (light red line). Two sets of data (inset) show a correlation of r=0.71.

compared to the unconstrained model, for a reasonable range of cut-off values the constrained model always shows better agreement with the experiment (Fig. 4). Figure 5 compares the mean square fluctuations of OmpF porin from x-ray experiment with our calculations for the best cut-off value, r_c =7.0 Å, and the spring constant c_b=0.002c. The calculated correlation coefficient in Fig. 5 is 0.72. Except at residues 110–130 which belong to the loop $L3$ in the OmpF constriction zone, both experimental and calculated mean square fluctuations follow the same trend. The sharp peak in the numerical results around loop $L3$ does not exist in the experiment. A similar peak has been also observed in MD simulation results by Watanabe *et al.* [33]. According to our results the loop $L3$ peak was highly sensitive to the choice of the cutoff. Specifically for a slightly larger cut-off value, r_c =7.2 Å, the peak disappeared resulting in an excellent agreement between the experiment and calculations (Fig. 6). However, increasing the cutoff reduced the overall performance and resulted in a slightly lower correlation coefficient of 0.71. Increasing the cut-off distance even further, forced the $L3$ loop to follow the less fluctuating corresponding experimental data, whereas it had destructive effects on the previously coinciding regions of the two plots.

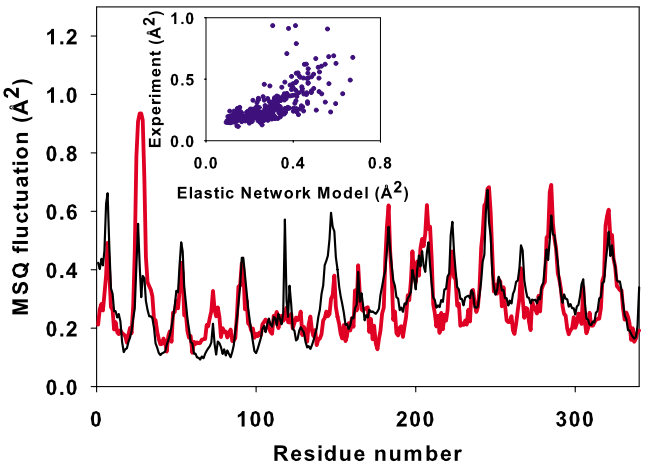

FIG. 5. (Color online) Mean square fluctuations, $\langle \Delta r_i^2 \rangle$, for constrained elastic network model with r_c=7.0 Å (dark black line) and the experimental values (light red line). Two sets of data (inset) show a correlation of r=0.72.

B. Specific porins

Specific porins are trimeric structures comprised of 18β-stranded barrels. The outer wall of these proteins starts from β8 and goes through β16 for each monomer. For this group of Omps, also, constraining the outer wall of the protein with additional springs results in better agreement between the numerical values from the modified elastic network model and the crystallographic experimental data, with even a small spring constant. By increasing the spring constant the results become insensitive to this parameter, and the correlation coefficient approaches a constant value. For this group, c_b=0.005c improves the correlation coefficient for 67% of porins in this group and the average of the values of best c_b for each porin in this group is 0.0037c. The results are summarized in Table I.

C. Transport Omps and poreless Omps

Porins of these group are constituted of monomeric β-stranded structures. The monomeric structures of these porins lead us to consider the whole strands as outer wall of porin connected with the membrane bilayer. For these groups, the constrained network shows smoother fluctuations and improved correlation coefficients. For transport Omps, the results show that c_b=0.001c improves correlation coefficients for 75% of the porins in this group and the average of the values of best c_b for each porin in this group is 0.0025c. For poreless Omps, c_b=0.004c improves correlation coefficients well for 83% of the porins in this group, and the average of the values of best c_b for each porin in this group is 0.0047c. The results for these Omps groups are also presented in Table I.

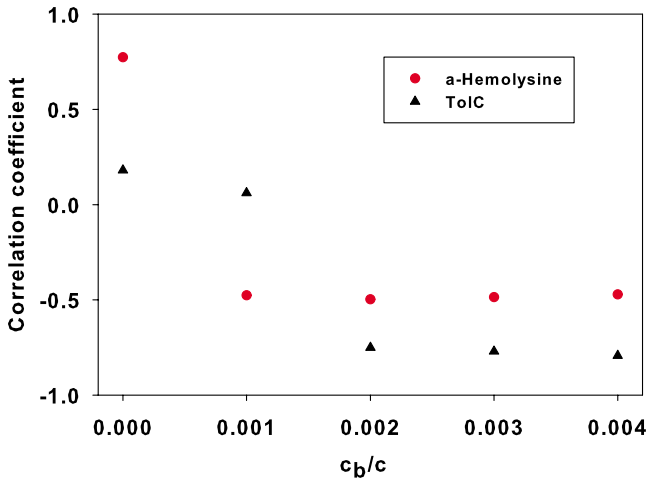

FIG. 7. (Color online) The correlation coefficient between the x-ray experimental data and the constrained elastic network model calculations of mean square fluctuations for composed pores at different spring constant ratios. The cut-off distance was taken as 8.0 Å in the calculations.

D. Composed pores

The porins of the last group are structurally different from other Omps. Adjacent β strands in the former groups are connected via a flexible loop but in composed porins, they are connected through more complex structures. They are connected by a long α-helix in TolC and combination of loops and β strands in α-hemolysin. Quite different structures of these porins, may causes quite different behavior for the correlation coefficient of computed results with experimental values in comparison with the other groups of Omps. For these porins, constraints, have diverse effects on correlation coefficients. (Fig. 7)

IV. DISCUSSION

By using a modified elastic network model, we have shown that the normal mode analysis of outer membrane porins successfully predicts the protein residues fluctuations well when compared to the experimentally measured mean square fluctuations. Experimental methods such as nuclear magnetic resonance and x-ray crystallography just measure the collective fluctuation over different modes. However, our theoretical method gives directly all modes and averages them to obtain the best correlation coefficients with experimental results. Also, it is significantly faster than time consuming methods such as MD. In our model, we only considered the C_α atoms in residues as point masses and represent their interactions by harmonic springs. In order to modify an elastic network model, considering a very weak interaction between the protein and the membrane, dramatically improves our results. The results show that $c_b=0.002c$ improved correlation coefficient for 67% of all studied Omps. Although the interactions between the protein and membrane are considered to be three orders of magnitude weaker than the inter-residue interactions, the improvement in the results is significant.

According to our results for a set of 22 available structure of bacterial outer membrane porins classified in five groups, the proposed elastic network model with only 2 parameters, can predict the dynamic behavior of these proteins very well (Table I). The results especially showed a good agreement with experiment for the loop $L3$ in the constriction zone of the general porins, especially at larger values of the cut-off distances. This suggests that the loop $L3$ must be interacting with some of the barrel residues at longer distances. This could be because of a hydrogen bond network [43], water crystals [33], or salt bridges [44], which were suggested before. Looking at the crystal structure of the protein, one can find that charged amino acids located on the $L3$, Asp 107, Asp 113, Glu 117, Asp 121, and Arg 100, are facing to the charged ones situated on the barrel wall, Arg140 and Asp126. But with regards to the distance between them, the only interacting ones found to be Arg 100-Asp 127 and Asp 107-Arg140. The former pair is located at the beginning of $L3$ that is not the subject of $L3$ Barrel wall interaction. However, the later one, that is located in the mid height of the channel, may cause an interaction between the barrel and midpoint of $L3$. Thus, the arrangement of these two amino acids might let a weak hydrogen bond to form, however, its affect still does not significantly change the range of the interactions we have calculated. Three other groups, including specific porins, transport Omps and poreless Omps, show also dramatic improvement in the results when the outer wall residues are constrained. The composed pores are the only group where considering membrane interactions does not improve the results and it shows diverse effects in the prediction of residues fluctuations. This could be related to the shorter structure connecting consecutive β strands instead of more flexible loops in the other porins.

In short, we developed a method for coarse-grained normal mode analysis based on an elastic network model with 2 parameters. This method, impressively enhances the correlation coefficient between computed results and available crystallographic experimental data for Omps comprised of antiparallel β strands connected through flexible loops.

ACKNOWLEDGMENTS

We thank H. Amirkhani for insightful conversations and her valuable comments on the draft manuscript. M.R.E. thanks the Center of Excellence in Complex Systems and Condensed Matter (CSCM) for partial support.

[1] F. B. Bass, P. Srop, M. Barclay, and D. C. Rees, Science **298**, 1582 (2002).
[2] G. E. Schulz, in *Protein Science Encyclopedia*, edited by A. R. Fersht (Wiley, New York, 2008).
[3] J. Deisenhofer, O. Epp, K. Miki, R. Huber, and H. Michel, Nature (London) **318**, 618 (1985).
[4] M. S. Weiss and G. E. Schulz, J. Mol. Biol. **227**, 493 (1992).
[5] S. W. Cowan, T. Schirmer, G. Rummel, M. Steiert, R. Ghosh, R. A. Pauptit, J. N. Jansonius, and J. P. Rosenbusch, Nature (London) **358**, 727 (1992).
[6] A. Kreusch and G. E. Schulz, J. Mol. Biol. **243**, 891 (1994).
[7] R. Dutzler, G. Rummel, S. Albertí, S. Hernández-Allés, P. S. Phale, J. P. Rosenbusch, V. J. Benedi, and T. Schirmer, Structure **7**, 425 (1999).
[8] K. Zeth, K. Diederich, W. Welte, and H. Engelhardt, Structure **8**, 981 (2000).
[9] T. Schirmer, T. A. Keller, Y. F. Wang, and J. P. Rosenbusch, Science **267**, 512 (1995).
[10] J. E. W. Meyer, M. Hofnung, and G. E. Schulz, J. Mol. Biol. **266**, 761 (1997).
[11] D. Forst, W. Welte, T. Wacker, and K. Diederichs, Nat. Struct. Biol. **5**, 37 (1998).
[12] K. P. Locher, B. Rees, R. Koebnik, A. Mitschler, L. Moulinier, J. P. Rosenbusch, and D. Moras, Cell **95**, 771 (1998).
[13] S. K. Buchanan, B. S. Smith, L. Vienkatramani, D. Xia, L. Esser, M. Palnitkar, R. Chakraborty, D. van der Helm, and J. Deisenhofer, Nat. Struct. Biol. **6**, 56 (1999).
[14] A. D. Ferguson, R. Chakraborty, B. S. Smith, L. Esser, D. van der Helm, and J. Deisenhofer, Science **295**, 1715 (2002).
[15] D. P. Chimento, A. K. Mohanty, R. J. Kadner, and M. C. Wiener, Nat. Struct. Biol. **10**, 394 (2003).
[16] A. Pautsch and G. E. Schulz, Nat. Struct. Biol. **5**, 1013 (1998).
[17] J. Vogt and G. E. Schulz, Structure **7**, 1301 (1999).
[18] H. J. Snijder, I. Ubarretxen-Belandia, M. Baauwi, K. H. Kalk, H. M. Verhij, M. R. Egmond, N. Dekker, and B. W. Dijkstra, Nature (London) **401**, 717 (1999).
[19] L. Vandeputte-Rutten, R. A. Kramer, J. Kroon, N. Dekker, M. R. Egmond, and P. Gros, EMBO J. **20**, 5033 (2001).
[20] S. M. Prince, M. Achtman, and J. P. Derrick, Proc. Natl. Acad. Sci. U.S.A. **99**, 3417 (2002).
[21] L. Vandeputte-Rutten, M. P. Bos, J. Tommassen, and P. Gros, J. Biol. Chem. **278**, 24825 (2003).
[22] L. Song, M. R. Hobaugh, C. Shustak, S. Cheley, H. Bayley, and J. E. Gouaux, Science **274**, 1859 (1996).
[23] V. Koronakis, A. Scharff, E. Koronakis, B. Luisi, and C. Hughes, Nature (London) **405**, 914 (2000).
[24] D. Ho, S. Chang, and C. D. Montemagno, Nanomedicine **2**, 103 (2006).
[25] B. Eisenberg, Proc. Natl. Acad. Sci. U.S.A. **105**, 6211 (2008).
[26] M. Chen, S. Khalid, M. S. P. Sansom, and H. Bayley, Proc. Natl. Acad. Sci. U.S.A. **105**, 6272 (2008).
[27] E. Z. Eisenmesser, O. Millet, W. Labeikovsky, D. M. Korzhnev, M. Wolf-Watz, D. A. Bosco, J. J. Skalicky, L. E. Kay, and D. Kern, Nature (London) **438**, 117 (2005).
[28] B. Brooks and M. Karplus, Proc. Natl. Acad. Sci. U.S.A. **82**, 4995 (1985).
[29] Q. Cui and I. Bahar, *Normal Mode Analysis: Theory and Applications to Biological and Chemical Systems* (CRC Press/Taylor & Francis Group, New York, 2006).
[30] I. Bahar, T. R. Lezon, A. Bakan, and I. H. Shrivastava, Chem. Rev. **110**, 1463 (2010).
[31] M. M. Tirion, Phys. Rev. Lett. **77**, 1905 (1996).
[32] A. R. Atilgan, S. R. Durell, R. L. Jernigan, M. C. Demirel, O. Keskin, and I. Bahar, Biophys. J. **80**, 505 (2001).
[33] M. Watanabe, J. Rosenbusch, T. Schirmer, and M. Karplus, Biophys. J. **72**, 2094 (1997).
[34] M. R. Ejtehadi, S. Avall, and S. S. Plotkin, Proc. Natl. Acad. Sci. U.S.A. **101**, 15088 (2004).
[35] M. K. Kim, G. S. Chirikjian, and R. L. Jernigan, J. Mol. Graphics Modell. **21**, 151 (2002).
[36] A. J. Rader, C. Chennubhotla, L. W. Yang, and I. Bahar, in *Normal Mode Analysis: Theory and Applications to Biological and Chemical Systems*, edited by Q. Cui and I. Bahar (CRC Press/Taylor &Francis Group, New York, 2006).
[37] J. L. Jeong, Y. Jang, and M. K. Kim, J. Mol. Graphics Modell. **24**, 296 (2006).
[38] B. Shanmugavadivu, H. J. Apell, T. Meins, K. Zeth, and J. H. Kleinschmidt, J. Mol. Biol. **368**, 66 (2007).
[39] T. Surrey, A. Schmid, and F. Jähnig, Science **35**, 2283 (1996).
[40] L. Yang, G. Songa, and R. L. Jernigana, Proc. Natl. Acad. Sci. U.S.A. **106**, 12347 (2009).
[41] R. S. Cantor, J. Phys. Chem. B **101**, 1723 (1997).
[42] W. R. Pearson and D. J. Lipman, Proc. Natl. Acad. Sci. U.S.A. **85**, 2444 (1988).
[43] A. Karshikoff, V. Spassov, S. W. Cowan, R. Ladenstein, and T. Schirmer, J. Mol. Biol. **240**, 372 (1994).
[44] K. M. Robertson and D. P. Tieleman, FEBS Lett. **528**, 53 (2002).